Multi-Phase Turbulent ISM: Theory Confronting Observations

Guang-Xing Li, MPIfR Bonn
Advisors : Nicolas Peretto, CEA Saclay, Patrick Hennebelle, ENS Paris

September 9, 2011

Abstract

In this document, we report our recent study on the turbulence inside the multi-phase ISM. First, we quantify the turbulence inside the molecular phase ISM by adopting a pixel-by-pixel line fitting strategy and studying the statistics of the fittings results of the ^{13}CO lines. The histogram of the ^{13}CO line amplitude and ^{13}CO line FWHM show power-law behavior, indicative of turbulence. Especially, the histogram of the FWHM of the ^{13}CO line show a $\mathrm{dN}/\mathrm{d}\sigma \sim \sigma^{-2.45}$ at high velocity end, which seems to be universal. By plotting the 2D histogram of the ^{13}CO line strength versus the ^{13}CO line width, a lower limit of the ^{13}CO line width for a given ^{13}CO line strength can be identified. We argue that such a lower limit is due to the self-gravity of the molecular cloud. Second, with the combination of ^{13}CO data from the GRS survey and the H I 21cm data from the VGPS survey, we study the connection between the molecular gas probed with the ^{13}CO line emission and the cold H I gas probed by the H I 21cm self-absorption feature. We found that the H I gas that is associated with the molecular clouds is also turbulent. The molecular clouds that have detectable H I envelope are more turbulent than clouds that do not show such envelope. Our results support the idea the molecular cloud turbulence is driven from outside, e.g. by the large-scale converging flow.

1 Introduction

The formation of molecular cloud is a key step in the formation of the stars. The molecular clouds typically have density range from (10^2 to $10^5\mathrm{cm}^{-3}$) and temperature range from 10-50 K. The major content of the molecular cloud is the H_2 molecule. Due to the fact that it is usually to difficult to excite the H_2 at such a low temperature, the molecular cloud is usually traced with the molecules like the CO molecule together with its different carbon and oxygen isotopes, and other molecules such as the NH_3 (ammonia).

Theoretically, such molecular gas can be formed out of the interstellar medium of the cold neutral phase (cold neutral medium, CNM), and it is speculated that the CNM can be form out of the hot H I gas with $T \sim 10^4 K$ (warm neutral medium, WNM) thought dynamically-triggered thermo-instability (Hennebelle & Pérault, 1999; Audit & Hennebelle, 2005). In such a case, the interstellar medium is both two-phase (CMN and WMN) and turbulent. However, only few evidences have been identified about the conversion of WNM to CNM (e.g. Nguyen Luong et al., 2011), and then to the molecular gas.

Molecular clouds are the nursery of the stars. While the formation of the molecular cloud can be explained by the conversion from WNM to CNM, how stars form in the molecular cloud is also an open question in astrophysics. It is found observationally that the kinematic structure of the molecular cloud is dominated by random motions with the characteristic speed much larger than the local sound speed. Such random motion is usually interpreted as turbulence. It is speculated that the formation of the stars inside the molecular cloud are control by such turbulence (Klessen, 2011, and references therein). The origin of the turbulence (random motion) is not well known. Interestingly, recent observational studies do suggest that the turbulence is driven from the large scale which is outside the molecular cloud (Klessen, 2011).

During the past years, the understanding of the star formation process have been greatly advanced by the employment of numerical simulations. The belief that the star formation process is controlled/regulated by supersonic turbulence have also been supported by such simulations. In this project, we confront the current observations of the molecular gas and CNM with simulations by Henebelle et al. in prep, and if the structure of the molecular gas and CNM can be explained by considering a two-phase turbulent interstellar medium model.

The aim of the project is two-fold. First, we aim to quantify the turbulence in the observed molecular cloud as well as in the numerical simulations, and second, we aim to explore the connection between the CNM and WNM.

To study the interstellar turbulence, we choose to use the ^{1}3CO data from the GRS galactic ring survey (Jackson et al., 2006) that was carried out using the FCRAO (Five College Radio Astronomy Observatory) 14m telescope. The observation covers the galactic place range of $l = 18$ deg-55.7 deg and a latitude range of $|b| < 1$ deg, a total of 75.4 square degrees with a resolution of ~ 1 arcmin using ^{13}CO line. The ^{13}CO have long been used as a tracer of the interstellar medium in the molecular phase, due to is large abundance and appropriate critical density. Analysis of the ^{13}CO data set will give us information of the turbulent motion of the molecular cloud down to sub-PC scale. Proper methods are needed to gain insights into the turbulence from the data. Method like (Lazarian & Pogosyan, 2000) can provide constraints on turbulence based on position-position-velocity (PPV) data cube. Delta-variance method (Ossenkopf & Mac Low, 2002) is another method that is widely employed in studying the turbulence, mainly due to its simplicity. Other methods that are also applicable, such as PCA (Heyer & Schloerb, 1997) and velocity centroid (Levrier, 2004). Second, we aim to explore the connection between CNM and molecular cloud, and shed light on the formation of the molecular cloud. In this project, we will try to constrain the turbulence based on the pixel-by-pixel Gaussian fitting the PPV data cube.

To explore the relation between the WNM and the CNM, we also use the H I data in the VGPS survey (Stil et al., 2006). The VGPS survey have good velocity resolution (< 1 km/s) and a angular resolution that is comparable to the GRS survey, making the analysis relatively easy. In the VGPS data, the WNM will appear as emission and the CNM will appear as absorption against the bright emission background (Li & Goldsmith, 2003; Gibson et al., 2005).

2 Quantifying the Turbulence in the Molecular Cloud

First we attempt to quantify the turbulence in the molecular cloud. What we have is the data cube of the ^{13}CO line emission. Inside the cube, the emission is function of the position (x,y) and the velocity v. We do line fitting in a pixel-by-pixel way.

1. Smooth the spectra with a smoothing length of 5 pixels in the velocity direction.
2. Find peaks that above a threshold, e.g. 0.3 K.
3. Fit the spectra with a sum of different Gaussian

$$s = g1(\mu_1, \sigma_1, A_1) + g2(\mu_2, \sigma_2, A_2) + ... + gn(\mu_n, \sigma_n, A_n) \tag{1}$$

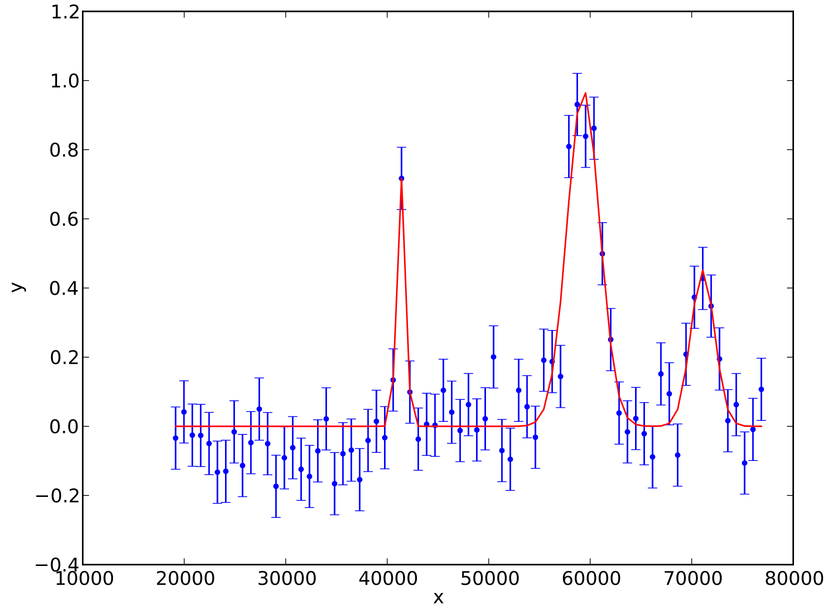

Figure 1: Example of a ^{13}CO line fitting.

Figure [1] shows an example of ^{13}CO line fitting.

The next step is to do statistics using the ^{13}CO lines. The simplest way is to the histogram of the velocity FWHM.

2.1 Cloud Properties

We choose G047.54-00.36 (Fig. [2]) as an example, and try to quantify the turbulence inside the cloud. Here is a brief summary of the property of the cloud.

1. Cloud Name:
   G047.54-00.36

2. Velocity:
   47.54 Km/sec

3. Kinematic Distance:
   3.6 Kpc

This is one of the clouds that are shown to have H I absorption lines that are associated with ^{13}CO emission. This is evident from the image of the cloud (figure [2]).

2.2 CO line statistics

Position-Position-Velocity Distribution of the of ^{13}CO line

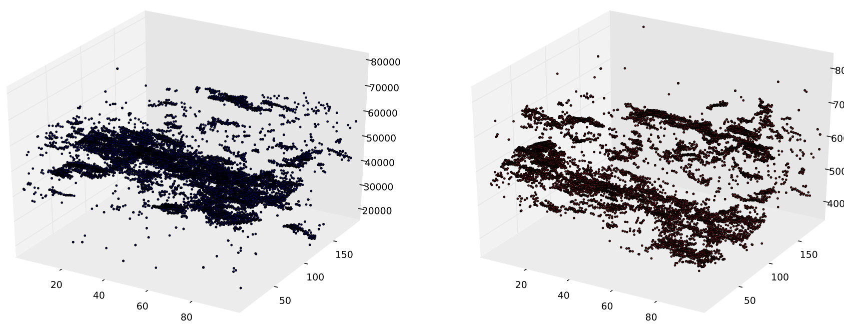

Figure 3: Position-Position-Velocity distribution of centroids of the ^{13}CO emission. The left panel shows the distribution of the centroids of the ^{13}CO emission line that is found to be associated with the H I emission, and the right panel shows the distribution of centroids of the ^{13}CO emission that is not found to be coincide with H I. The conclusion that can be draw from this plot is that the whole cloud that we are looking at (the central part of the cube) is mixed with cold H I gas.

Before we start, it is worthwhile to have a look at the spatial distribution of the centroids of the ^{13}CO emission line that is picked out by our algorithm. Fig. [3] shows the distribution of the centroids of the ^{13}CO emission line in position-position-velocity space. The left panel shows the distribution of the peaks that is found to be associated with the H I absorption feature, and the right panel shows the distribution of the emission peaks that is not found to be associated with the H I absorption feature (see §3.1 for the details). Note that due to the complexity of the H I emission (emission, continuum absorption, and

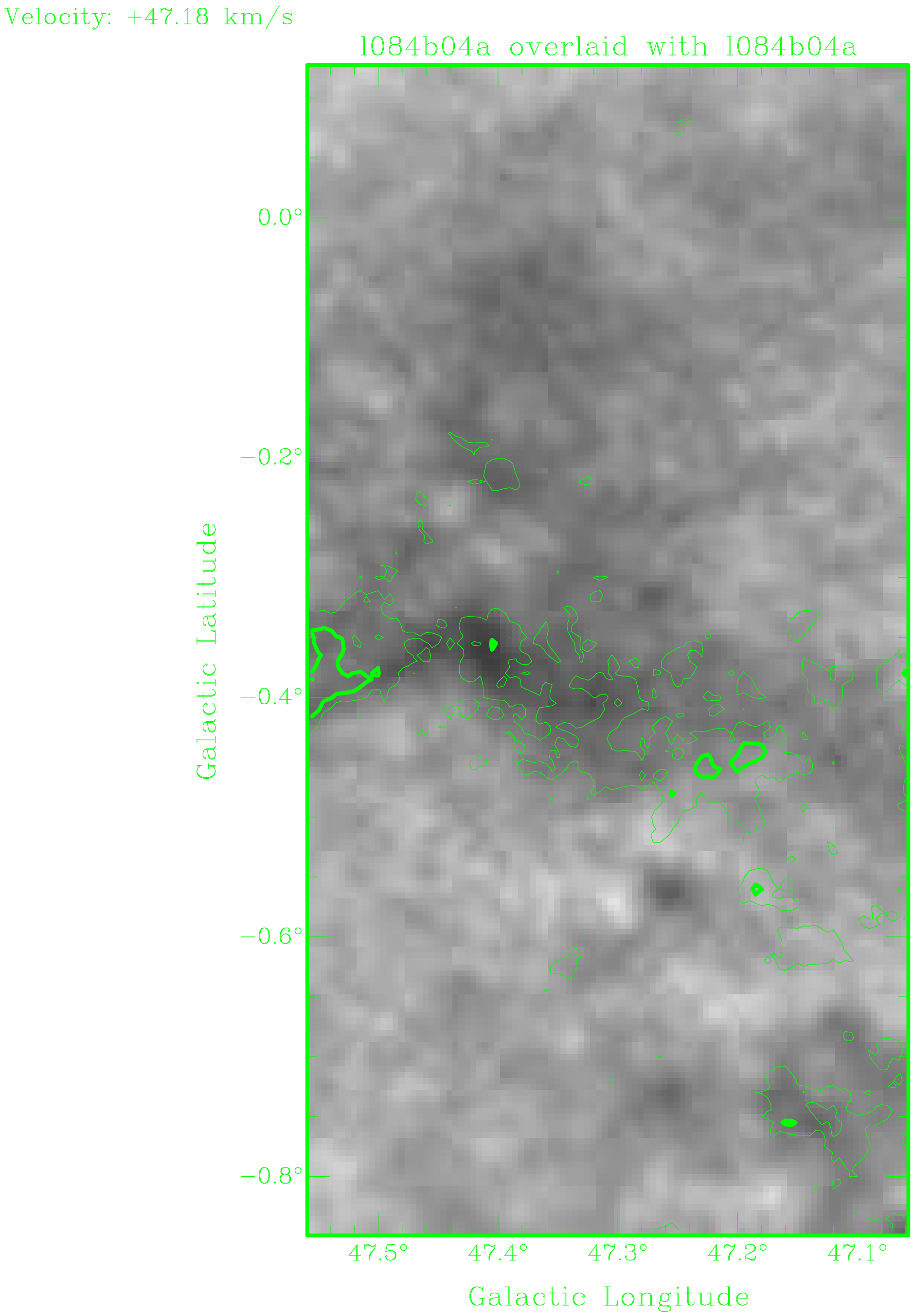

Figure 2: Morphology of cloud G047.54-00.36. The grey scale is the H I emission, and the green contours are the ^{13}CO(1-0) line emission. ^{13}CO T_{A*} contours start at 0.3 K in step of 0.3 K.

line self-absorption superimposed together), for some ^{13}CO emission peaks, it is difficult to tell if a H I absorption feature is present or not.

One important piece of information from this plot is that the whole cloud of interest (see the points at the central part of the left panel) is found to be associated with H I absorption feature. This indicate that in some cases the molecular gas is surrounded by/ mixed with cold atomic-phase H I gas. This supports the idea that molecular clouds are born in a turbulent sea of atomic gas, and strengthen the connection between the WNM and the molecular medium.

Velocity Distribution of the ^{13}CO line of the whole cube

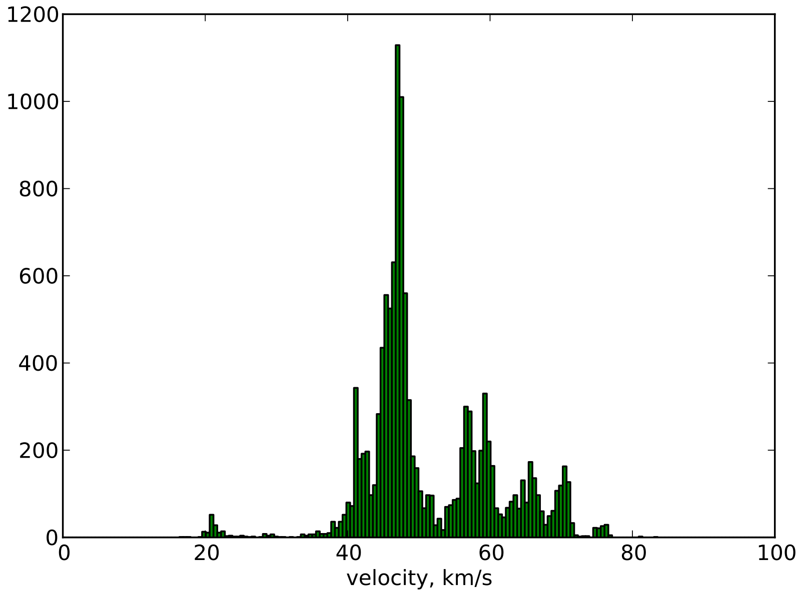

Figure 4: distribution of the velocity of the ^{13}CO lines of the whole cube.

In figure [4] we plot the distribution of the velocity of the ^{13}CO lines. Four main components can be identified from the figure. These four components correspond to four clouds that lies in our cube. The main cloud of interest have a velocity of ~ 47.54 km/s, and it correspond the first and highest peak in this plot.

Distribution of the ^{13}CO line amplitude

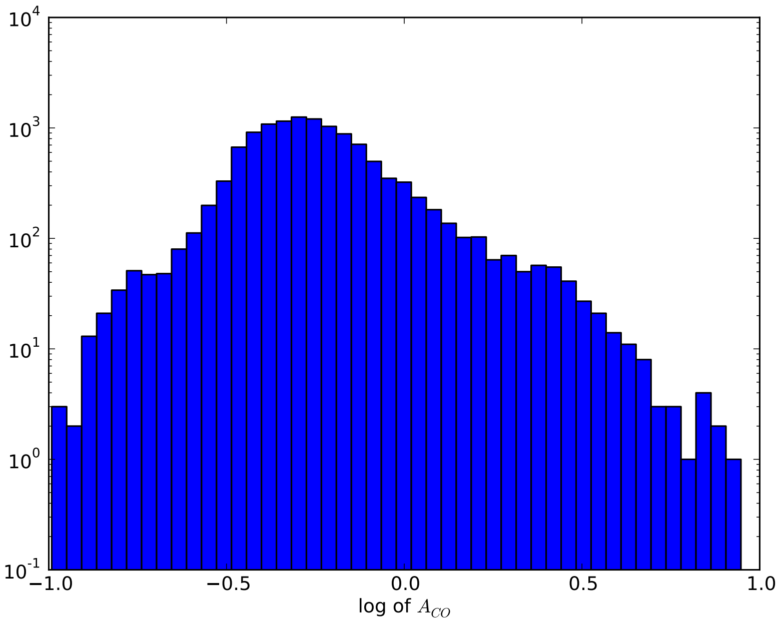

Figure 5: Histogram of ^{13}CO line strength. The horizontal axis is the logarithm of the amplitude of the ^{13}CO lines.

In figure [5] we plot the histogram of the amplitude of all the detected ^{13}CO lines. The distribution seems to be restricted by two power-laws lines. While the horizontal axis in Fig. [5] stands for the amplitude of the ^{13}CO lines, the larger the A is, the larger the column density is. So the contribution at the high-A side comes mainly from large clumps, and the contribution of the low-A side comes mainly from small clumps. This is consistent with the picture that the clumps have a pow-law mass distribution. At the left part of the plot, there is trend that the smaller the A, the smaller the number of components. This may due to detection limit.

Distribution of the ^{13}CO line width

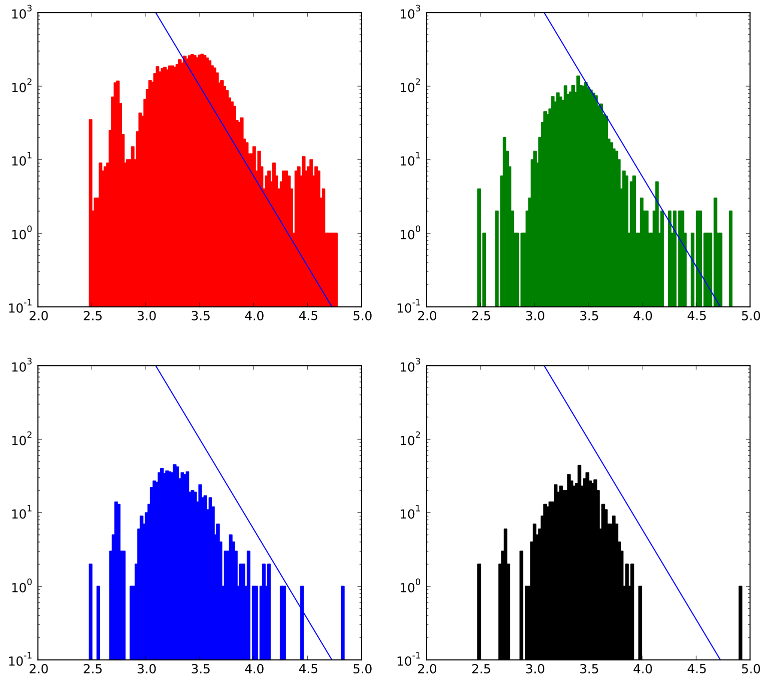

Figure 6: Histogram of the logarithm of the full-width-half-maximum of the ^{13}CO lines. The horizontal axis is the log of the FWHM of the ^{13}CO lines, in unit of cms^{-1}. Here we plot the histogram of the four different cloud, respectively (see Fig [4]). The four clouds that can be identified in figure [4] is denoted by red, green, blue and black colors, respectively. In each panel, the blue line is the plot for $\frac{\mathrm{dN}}{\mathrm{d}\sigma} \sim \sigma^{-2.45}$.

Figure [6] shows the distribution of the ^{13}CO line width of the four sub-clouds. The central velocity of the four clouds can be identified in Fig [4]. Despite the possible contaminations that may be contained in each component, a universal slope of $\frac{\mathrm{dN}}{\mathrm{d}\sigma} \sim \sigma^{-2.45}$ can be identified at the right hand-side of the histogram. Such a slope is indicative the existence of universal turbulence amount the different clouds.

Correlation between the ^{13}CO line width and the ^{13}CO line strength
Figure [7] shows the correlation between the ^{13}CO line width and the ^{13}CO line strength. This is the 2D histogram, with the color denotes the number density of the components that falls into the bin. If we project the plot onto the X direction, we get the histogram of the line amplitude, and if we project this plot onto the Y direction, we get the histogram of the line width. Two trends can been seen from the plot. First, with the increase of the line strength, the line width tends to be smaller. This may because the larger the line width

is, the denser the region is. Such dense regions usually have small spatial extent, which correspond to small velocity. Second, with the increase of the line strength, there seems to be an lower limit of the line width. This may because of the self-gravitating motion inside the clump. When we look at the very strong ^{13}CO lines, we look at the region with high density. When the region, is dense enough, the self-gravity becomes important. Such self-gravity can give rise to a finite line width. This trend can be explained by considered the following scaling:

$$\rho_{core} \sim const \tag{2}$$

$$m_{core} \sim \rho_{core} l_{core}^3 \sim l^3 \tag{3}$$

$$\sigma \sim \sqrt{\frac{GM}{r}} \sim l \tag{4}$$

$$A_{co} \sim \frac{m}{\sigma} \sim l^2 \tag{5}$$

$$\sigma \sim A_{co}^{1/2} \tag{6}$$

See figure [8].
We are planning to apply this diagnostics plot to all the clouds in the GRS survey.

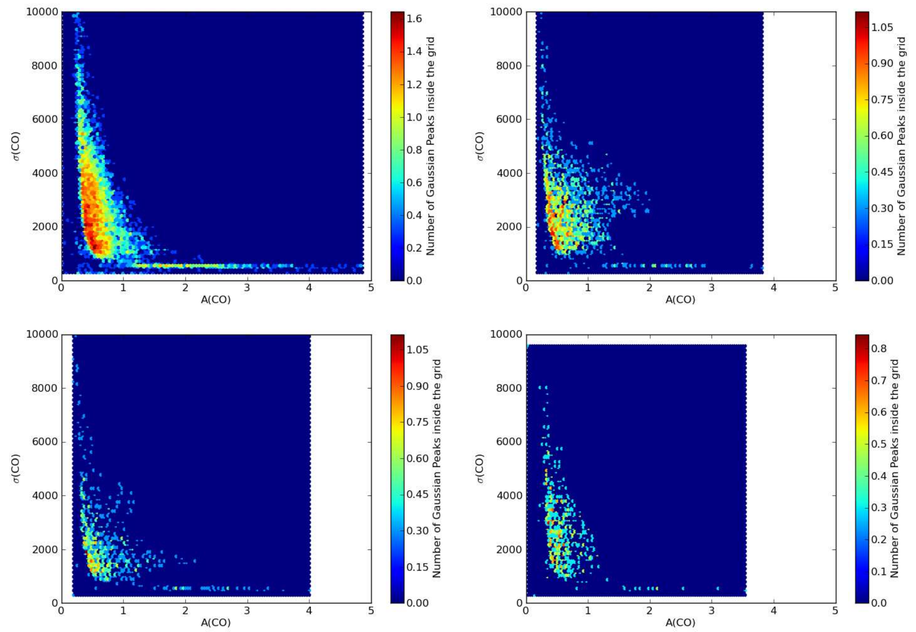

Figure 7: 2D histograms of the ^{13}CO line. The horizontal axises are the amplitude of the ^{13}CO line, and the vertical axises are the FWHM of the ^{13}CO line. The color stand for the number density of the ^{13}CO line in each bin. The four panels stands for the four clouds that can be identified in Fig. [4]

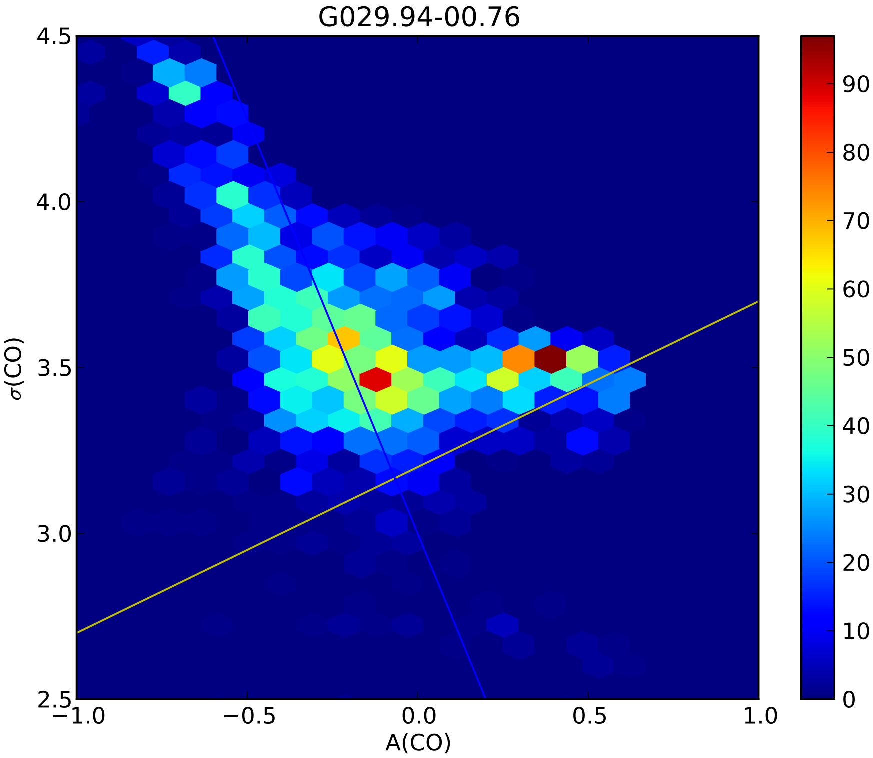

Figure 8: 2D histogram of the ^{13}CO line for cloud G029.94-00.74. The yellow line is from the scaling of Eq. [6].

3 The relation between molecular gas and CNM

The molecular gas is traced conveniently using ^{13}CO, and CNM gas are traced using H I absorption feature on background H I emission and background centimeter continuum. The VGPS H I data is more irregular than the GRS ^{13}CO data, because the H I emission, the H I absorption against the background continuum and the H I absorption against the emission are superimposed together. We use the source catalogue from GRS survey, and use it as a starting point to look into the connection between the CNM and molecular gas. We aim to look at the connection between the ^{13}CO gas and the cold H I gas. In order to find the clouds that have the association between the ^{13}CO and the H I , we write a routine to go through all the clouds. Fig. [9] show screenshot of our program. The top left panel shows the ^{13}CO cloud. If the cloud have ^{13}CO-HI association, we can see a corresponding absorption feature in the upper left H I emission plot.

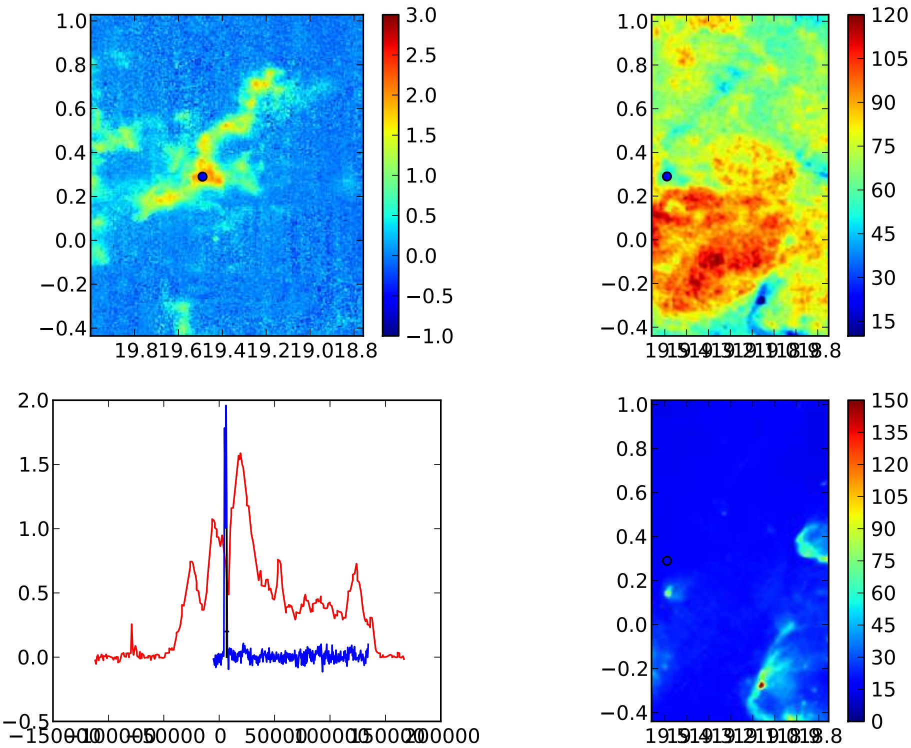

Figure 9: Screenshot of the interface of our subroutine that is used to go through all the GRS clouds. Upper left: CO emission for a given velocity channel. Center of the source is denoted as a dot. Upper right: H I emission for the same velocity channel. Center of the source is denoted as a dot. Lower Left: Spectra for the CO data and the H I data. The red line is the HI spectra at the central of the source (dot position), and the blue line is the CO spectra (the H Iflux have been scaled to the flux of the ^{13}CO line). Lower Right: Centimeter continuum emission. The cloud shown in this plot is a cloud where the CO emission is related to the HI absorption.

3.1 HI line fitting

Having identified the clouds where CO emission and H I absorption features are associated, we try to quantify the H I self-absorption feature. The H I spectra is more difficult to interpret than the ^{13}CO spectra, because what we actually see is the superposition of emission and absorption features. Guided by the ^{13}CO line emission, we try to interpret the H I data. What we did is as follows:

1. Restrict the velocity range so that the spectra have a relatively simple shape, e.g. with a relatively well-defined baseline and some absorption features.

2. Use a seven-order polynomial to fit the H I spectra (*Note: Such a fitting strategy tend to overlook the broad absorption features).*

3. Check the residual of the fit. The residual are the possible absorption caused by the cold H I gas. When the residual is larger than 6K, we add a Gaussian component to take the absorption into account. The final form of the spectra model is

$$s = p(c1, c2, c3, ..., c7) - g1(\mu_1, \sigma_1, A_1) - g2(\mu_2, \sigma_2, A_2) - .... - gn(\mu_n, \sigma_n, A_n)\ ; , \tag{7}$$

   where $p(c1, c2, c3, ..., c7)$ is the polynomial component, and $gi(\mu_i, \sigma_i, A_i)$ are the Gaussian components.

4. Re-run the fitting procedure, to measure the parameters of each Gaussian component.

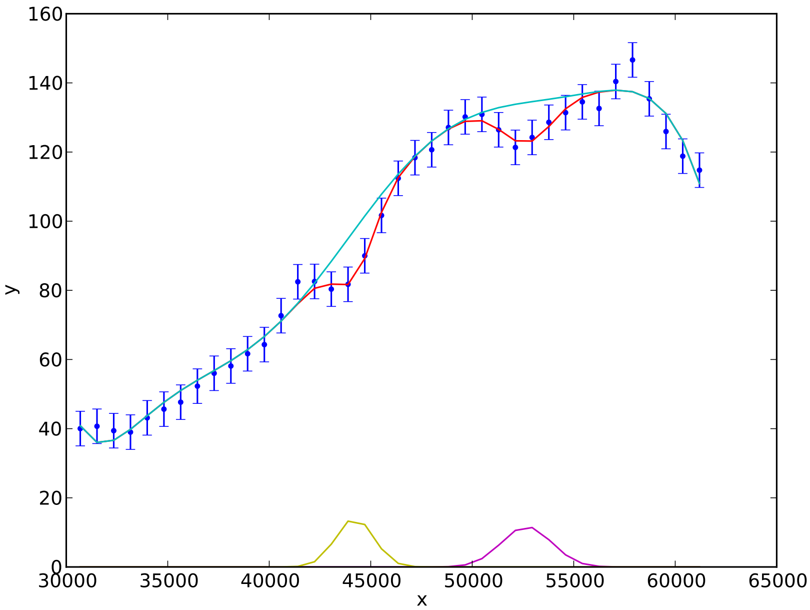

Figure 10: Example of the fitting of a H I spectra. The horizontal axis is the frequency (in terms of velocity), and the vertical axis is the flux (in unit of K). The red line the full model. The blue line is the polynomial component, and the yellow and pink lines are the two Gaussian feature that are identified by the algorithm.

After doing the fitting, we have two catalogues. The first one is the ^{13}CO line catalogue, which contains the following elements:

1. The spatial position of the ^{13}CO line (x,y).

2. The parameters of the ^{13}CO line (A, $v_{\rm cent}$, σ), where A is the amplitude of the ^{13}CO line, $v_{\rm cent}$ is the central velocity of the ^{13}CO line, and σ is the velocity FWHM of the ^{13}CO line.

The second catalogue is the H I line catalogue, which contains

1. The spatial position of the H I line (x,y).

2. The parameters of the H I line (A, $v_{\rm cent}$, σ), where A is the amplitude of the H I line, $v_{\rm cent}$ is the central velocity of the H I line, and σ is the velocity FWHM of the H I line.

We are interested in the H I absorption feature that is related with the ^{13}CO line emission. In order to achieve this, we cross-matched the two catalogues, and picked out the H I absorption features that are coincide with the ^{13}CO line in both spatial and velocity coordinates.

The criterion for the coincidence in velocity space is relatively simple: for the ^{13}CO lines we have the central velocity $v_{\rm CO}$ and the FWHM $\sigma_{\rm CO}$, and for the H I lines we also have the line central velocity $v_{\rm HI}$and the FWHM $\sigma_{\rm HI}$. For a given position, the two lines are coincide, if

$$v_{\rm HI} - \sigma_{\rm HI} < v_{\rm CO} < v_{\rm HI} + \sigma_{\rm HI} \tag{8}$$

or

$$v_{\rm CO} - \sigma_{\rm CO} < v_{\rm HI} < v_{\rm CO} + \sigma_{\rm CO} \; . \tag{9}$$

The following results are based on a catalogue that come from a cross-match between the ^{13}CO lines and the H I lines.

3.2 Relation between the ^{13}CO line and the H I line

Here I present the result from combining the ^{13}CO lines with the H I lines. In figure [11] we plot histogram of the H I line strength. The histogram of the ^{13}CO lines, which is associated with the H I absorption feature, is also plotted for comparison. One remarkable feature in this plot is the similarity between distribution of the amplitude of the ^{13}CO line and the distribution of the amplitude of the H I line. The similarity of the distribution may imply that the molecular gas and the cold H I gas have identical turbulent structure (in a statistical sense).

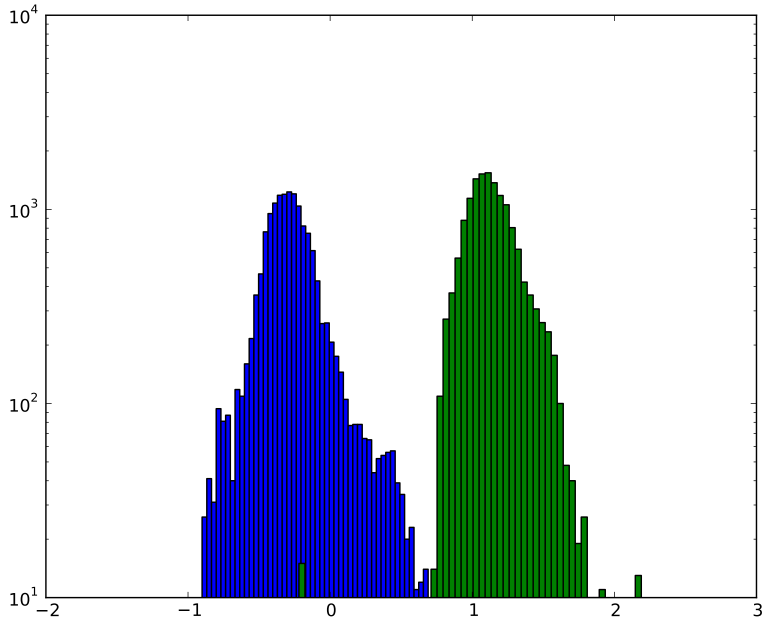

Figure 11: Histogram of the amplitude of the H I absorption feature. The H I histogram is plotted in green, and the ^{13}CO histogram is plotted in blue, for reference. Note the similarity between the two distributions.

H I line width

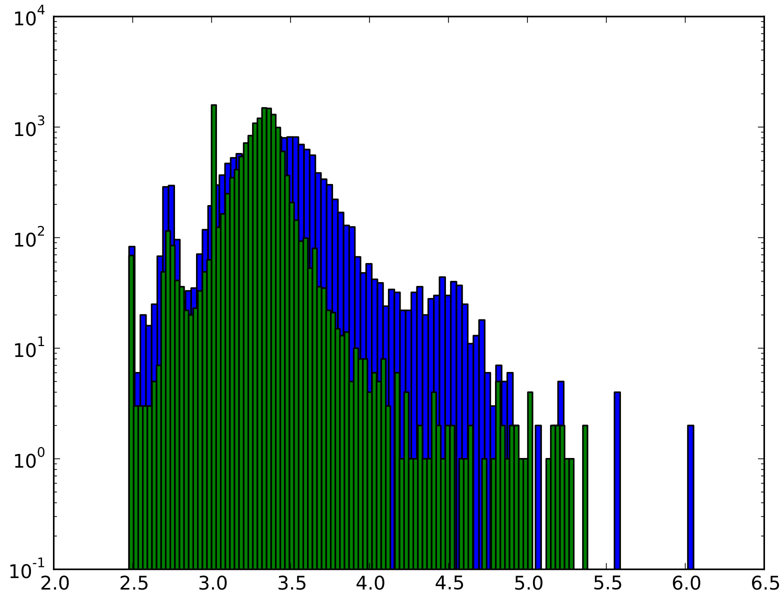

Figure 12: Histogram of the FWHM of the H I absorption feature. The histogram of the ^{13}CO emission line FWHM is also plotted for comparison. The Hi histogram is plotted in green, and the ^{13}CO histogram is plotted in blue.

Figure [12] shows the histogram of the FWHM of the H I absorption feature. For comparison, we plot the histogram of the amplitude of the ^{13}CO emission line. Two peaks can be found in the distribution. This because of the existence of narrow emission feature on top of broad emission features. One interesting feature is that the ^{13}CO lines have a broader distribution than the H I lines. Since ^{13}CO line trace the densest part of the molecular cloud, the fact that ^{13}CO lines tends to be broader than the H I line is maybe due to the reason that at the dense part of the molecular cloud the gravity becomes important, and the motion due to gravity contributes significantly to the observed line width.

H I line strength vs. H I line width
Fig. [13] shows the 2D histogram of the H I line strength and the H I line width. Different from the CO lines, for H I lines, the larger the line strength, the larger the line width. This may be because that larger H I line strength correspond to larger scale, which then correspond to larger velocity.

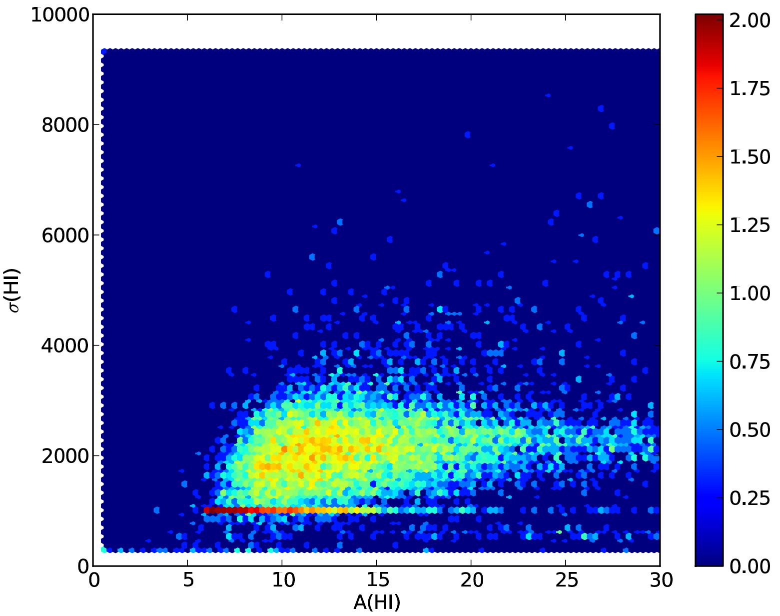

Figure 13: 2D histogram showing the relation between H I line strength and the H I line width. The horizontal axis is the H I line strength, and the vertical axis is the H I line width. Color stand for the density of points in a given region.

^{13}CO line strength vs. H I line strength

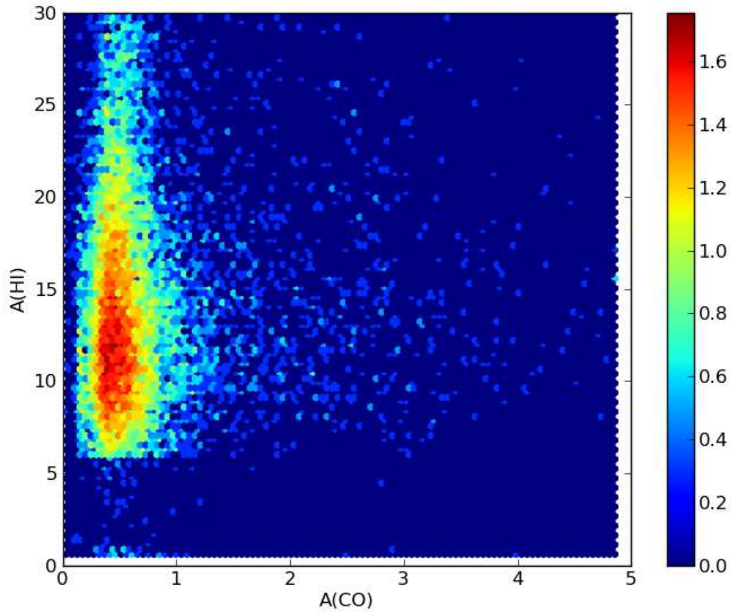

Figure 14: 2D histogram of the amplitude of the ^{13}CO emission line and the H I absorption feature.

Figure [14] plots the 2D histogram of the amplitude of the ^{13}CO emission line strength and H I absorption feature strength.

One remarkable information for this plot is the non-correlation between the ^{13}CO line and the H I line: given the fact that the H I envelope is spatially associated with the molecular cloud (traced by the ^{13}CO) and the fact that the ^{13}CO lines and the HI lines both show turbulent behavior, it is surprising to see that there is no correlation between the ^{13}CO line amplitude and the H I line amplitude. Fig. [15] shows the 2D histogram of the ^{13}CO line FWHM and the H I line FWHM. There is no correlation between them either.

Our conclusion from Fig. [14] and Fig. [15] is that ^{13}CO and H I tracer the cold condensation of the ISM. They belong to the same turbulence structure. However, they trace different part of the cloud (cold condensation). The similarity of the turbulence traced by the ^{13}CO and the turbulence traced by the ^{13}CO can by explained by the if the cloud turbulence is driven from outside, e.g. large-scale converging flow.

^{13}CO line width vs. H I line width

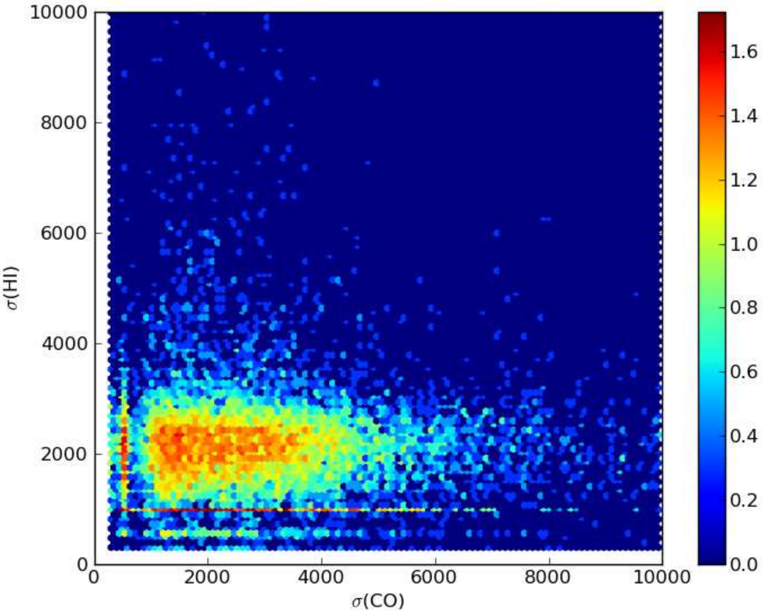

Figure 15: 2D histogram of the FWHM of the ^{13}CO emission line and the H I absorption feature.

4 Analysis of Spectra from Simulations

One major part of the project is to confront the simulations with the observations, and try to catch the signature of the turbulence. Similar to the observations, our simulation data also have the ^{13}CO part and H I part. However, it is difficult to analyze the H I data from the simulation, as the absorption feature is usually irregular, and the absorption is usually saturated. In this section, we will focus on the analysis of the ^{13}CO data from the simulation.

There are also some problems with the ^{13}CO data from the simulations. One major problem is that the ^{13}CO line emission is usually narrower than what is typically observed. As we will show in the following section, even though that the simulation have some problems, it still show some features that are comparable with observations.

4.1 Histogram of ^{13}CO line strength

Figure[16] shows the histogram of the ^{13}CO line strength.

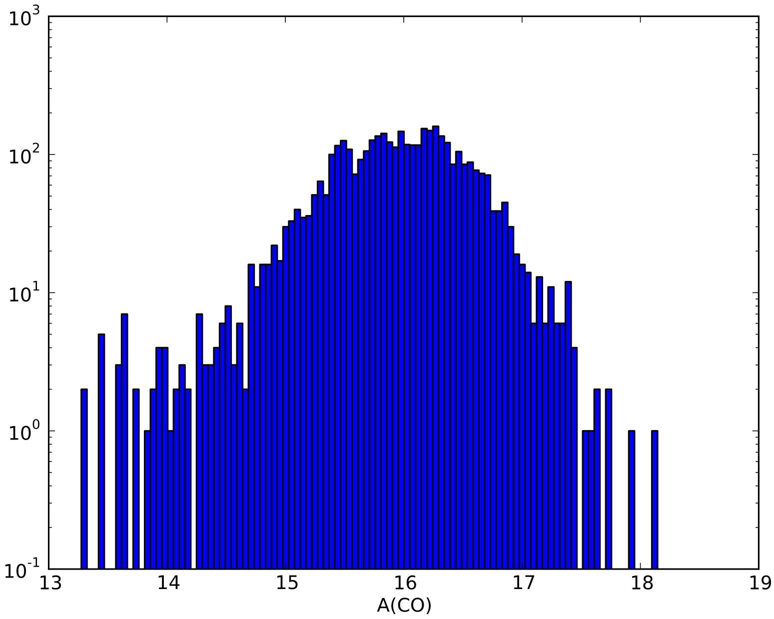

Figure 16: Histogram of ^{13}CO line strength from simulations. The x axis is the logarithm of the intensity of the ^{13}CO line. The scale of the x axis is not absolute.

4.2 Histogram of ^{13}CO line FWHM

Figure [17] shows the histogram of the ^{13}CO line FWHM. According to the plot, the ^{13}CO line can be very narrow in the simulations. This may be because of the fact that the internal motion from small scales (<0.1 pc) is not well resolved in the simulations. It is interesting to see that the relation $\mathrm{dN}/\mathrm{d}\sigma \sim \sigma^{-2.45}$, which is found in observations, can be identified in the simulations here.

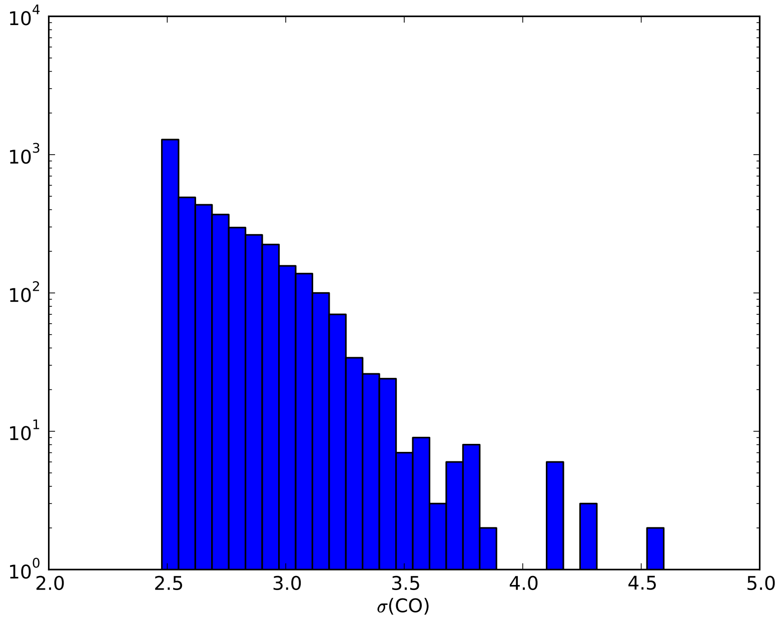

Figure 17: Histogram of ^{13}CO line FWHM from simulations. Note the unit of x label is in log scale.

4.3 2D histogram of ^{13}CO line amplitude and ^{13}CO line width

Fig. [18] shows the 2D histogram of the ^{13}CO lines from the simulation. The same of the case from observations, larger line strength correspond to smaller line width. However, the $\sigma \sim A^{1/2}$ (equation 6) limit can not be identified in this plot, probably due to the limited resolution of the simulation. In the future, we will try different simulations, in order to understand this difference.

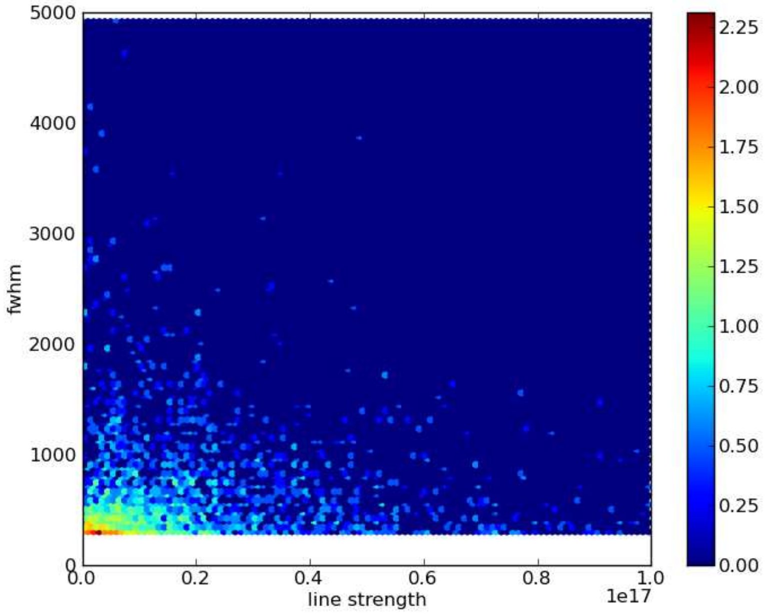

Figure 18: 2D histogram of ^{13}CO line strength and ^{13}CO line FWHM from the simulations.

To summarize, the ^{13}CO line statistics that we observe can not be well reproduced by this simulation. This may because the resolution of the simulation is not enough. The size of the whole simulation box is 500pc, and the effective resolution of the AMR simulation is $2^{11} \times 2^{11} \times 2^{11}$. Such a simulation have a resolution of about 0.24pc, which is roughly comparable to the size of a single pixel from the GRS observations. Thus, the internal motion inside each pixel is not well-resolved by the simulation. The fact that the ^{13}CO line width is artificially narrow may be just one manifestation of this limitation.

5 Are the turbulence driven from outside?

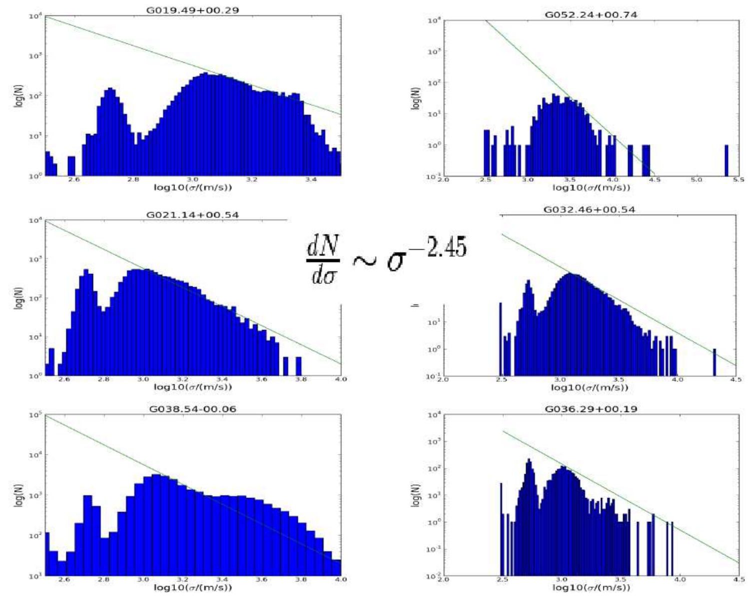

Figure 19: Histogram of FWHM of six sources from the GRS catalogue. The left panels are the plots for clouds that have CO-H I association, and the right panels are the plots for the clouds that do not have CO-H I association.

One important question concerning the turbulence inside the molecular cloud is the driving mechanism. Different driving sources have been proposed. One set of proposals is that the turbulence is driven from outside (Klessen, 2011). Another proposal is that the turbulence is driven from inside the molecular cloud, e.g. by the outflow from protostars.

In this work, we have made a distance-limited sample of clouds (d<1.5 Kpc). In this sample, we select clouds that have the association between ^{13}CO and H I, and also clouds that do not show detectable association between ^{13}CO and H I. We use our histogram of velocity FWHM to quantify the turbulence of the molecular cloud. If the high-velocity end of the histogram follows $dN/d\sigma \sim \sigma^{-2.45}$, we conclude that the cloud is turbulent. If the high-velocity end of the histogram show a slope which is steeper than -2.45, we conclude that the cloud is not so turbulent. Given the fact that we do not fully understand the slope, we use it as way to quantify the turbulence in the molecular cloud.

Fig. [19] shows the results. The three panels on the left side are the results for clouds that have the association between the ^{13}CO and the H I , and the three panels on the right side are the results for clouds that do not show association between the ^{13}CO and the H I . It can be seen that the clouds that have the ^{13}CO-HI association are more turbulent than the clouds that do not have such association. This may indicate that the turbulence is driven from outside, e.g. by the large-scale converging flow.

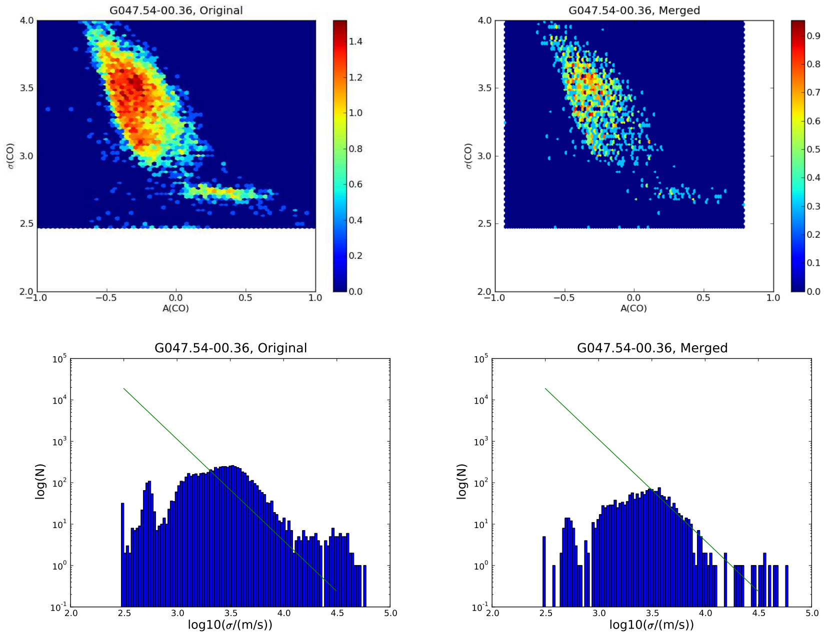

Figure 20: Comparison of the diagnostics plots between the original data and the data where four neighbouring pixels are merged. Upper Left: 2D histogram of amplitude and FWHM of the CO lines for the original data cube. Upper Right: Same as the upper left panel, but for the cube with every four neighbouring pixels merged together. Lower Left: Histogram of the CO line FWHM for the original data cube. Lower Right: same as the lower left panel, but but with the data cube where every four neighbouring pixels merged together.

6 Discussion

6.1 Are the results affected by the finite resolution of the telescope beam?

While our diagnostics plots can quantify the structure of the cloud, it is necessary to check whether our diagnostics plots are affected by the distance of the cloud. Since we can not find two identical clouds at different distances, we select one cloud, and put it at different distances, and see if the resulting diagnostic plots are similar.

The details are as follow: First, we select a cloud, and produce all the diagnostics that we are interested in. Then, we smooth the data cube by merging every four neighbouring pixels into one single pixel. This is equivalent to putting the cloud at a distance which correspond to two times of its original distance. Finally, we produce the same diagnostics plot for the smoothed data cube. Fig. [20] shows the results. After the smoothing, the number pixels is 1/4 of the original number. It turns out that the major feature that we are interested in such as the slope at the velocity FWHM histogram, the shape of the cloud seen in ^{13}CO line amplitude-CO line velocity FWHM plot are unchanged. We thus conclude that the our results are relatively unaffected by the distance.

7 Conclusion

In this project, we have developed a method that can quantify the turbulence motion and self-gravity inside the molecular cloud. We perform pixel-by-pixel line fitting of the ^{13}CO PPV data cube, and do statistics based on such fitting. The turbulence is seen as the power-law dependence of the number of Gaussian components on the amplitude of the ^{13}CO line, and the FWHM of the ^{13}CO line. The self-gravity can by identified by looking at the 2D histogram of the ^{13}CO line amplitude and the ^{13}CO line FWHM: for strong ^{13}CO lines, there exists a lower limit of the ^{13}CO line FWHM. The lower limit of the FWHM and the line strength are linked by $\sigma \sim A^{1/2}$, which can be derived by considering the self-gravity of the clumps inside the cloud.

Based on this method, we look into the connection between molecular cloud turbulence and the ^{13}CO-H I association. With ^{13}CO emission, we probe the dense part of the molecular cloud, and with H I self-absorption feature, we probe the cold H I envelope surrounding the molecular cloud. Our results suggest that for molecular clouds that are surrounded by cold H I envelope, the motion of the molecular gas is more turbulent than clouds without detectable cold H I envelope. The results support the idea that the turbulence of the molecular cloud is driven from outside, probably from the converging hot H I gas.

We will extend the work in several ways. First, since the current study of the trend in §5 is limited only to several sources, we would like to expand this study to the whole sample of GRS clouds. Second, we will try to quantify the association between the H I self-absorption feature and the ^{13}CO emission in a more quantitative way. Third, we will analyze a simulation with much higher resolution, in order to better resolve the densest region where gravity plays important role in determining the cloud dynamics. Hopefully, such an analysis will yield predictions which better match the observations.

It is also helpful to further compare our work with other studies that try to constrain turbulent motion from observations, and see what additional information can be obtained from our approach.

Acknowledgements
We thank Pascale Garaud, Doug Lin and all other organizers of 2011 ISIMA program, and thank the Kavli Institute for Astronomy & Astrophysics at Beijing for hosting the activities. Guang-Xing Li would like to thank Ralf Klessen, Nathan Goldbaum, Matthias Gritschneder, and other participants of ISIMA for helpful discussions and comments, and would like to thank Xun Shi for helpful comments on the manuscript. Guang-Xing Li's travel is supported by IMPRS (International Max Planck Research School) for Astronomy and Astrophysics at Bonn and Cologne.

References

Audit, E., & Hennebelle, P. 2005, A&A, 433, 1

Gibson, S. J., Taylor, A. R., Higgs, L. A., Brunt, C. M., & Dewdney, P. E. 2005, ApJ, 626, 195

Hennebelle, P., & Pérault, M. 1999, A&A, 351, 309

Heyer, M. H., & Schloerb, F. P. 1997, ApJ, 475, 173

Jackson, J. M., et al. 2006, ApJS, 163, 145

Klessen, R. S. 2011, ArXiv e-prints

Lazarian, A., & Pogosyan, D. 2000, ApJ, 537, 720

Levrier, F. 2004, A&A, 421, 387

Li, D., & Goldsmith, P. F. 2003, ApJ, 585, 823

Nguyen Luong, Q., et al. 2011, A&A, 529, A41

Ossenkopf, V., & Mac Low, M.-M. 2002, A&A, 390, 307

Stil, J. M., et al. 2006, AJ, 132, 1158